Stochastic Wave Radiation by the Gulf Stream*

NELSON G. HOGG

Woods Hole Oceanographic Institution, Woods Hole, Massachusetts

(Manuscript received 28 January 1988, in final form 27 May 1988)

ABSTRACT

A linear, small amplitude model of Rossby waves forced by idealized meanders is presented in order to ascertain whether or not the observed low frequency motions near the Gulf Stream are capable of being so generated. Two crucial ingredients are shown to be necessary; the meandering activity must vary in the downstream direction and the meanders must have a transient behavior. Cast as a stochastic average over a large number of meanders the predicted amplitudes of the kinetic energy and Reynolds stresses are similar to those observed. Implications for the forcing of a mean flow are discussed.

1. Introduction

The dominant low frequency motions on the lower continental slope and rise of the western North Atlantic are energetic topographic Rossby waves. Various mechanisms have been explored for their generation, the most visually compelling being that of Louis and Smith (1982) who were able to reproduce a burst of motions at a mooring with a model of generation by a Gulf Stream ring.

Indeed, the Gulf Stream itself has been implicated as the source for these motions (Hogg 1981; Weatherly and Kelly 1985; Welsh et al. 1987). However, the dominant disturbances to the Stream are eastward propagating meanders from which it is difficult to radiate energy into Rossby wave motions which propagate westward (Pedlosky 1977; Talley 1983). In fact, such radiating motions must decay away from the source and have eastward phase propagation to match that of the assumed steady disturbance. The observed Rossby wave motions propagate westward (Hogg 1981; Price and Rossby 1982; Welsh et al. 1987) so this steady forcing mechanism is inappropriate.

Recent work (Welsh et al. 1987) has uncovered eastward moving disturbances in the deep Stream that could couple more directly to the far field wave motions. However, it is not clear what causes these motions or, indeed, whether they might be the response of the Stream to external motions.

Meanders are not steadily moving frozen features—they have a definite life cycle and, in their growth and decay periods, will force transient motions in the form of Rossby waves as in the ring model of Louis and Smith (1982). More recently, Malanotte-Rizzoli et al. (1987) have shown that pulsating meanders are also able to radiate Rossby wave energy provided that the pulsation frequency is low enough.

This paper considers a statistical or stochastic extension of the transient meander model with the objective of computing the far-field response to compare with the observed wave field. Although serious approximations must be made, in particular that motions are linear and small amplitude, the conclusion is reached that transient meanders are capable of producing observed kinetic energy and Reynolds stress distributions.

In the vicinity of the Gulf Stream downstream from Cape Hatteras these distributions have characteristic patterns which are very elongated in the downstream direction (Richardson 1983; Schmitz 1984; and Cheney et al. 1982). Cross-stream structure at 55°W in the North Atlantic is shown in Fig. 1. The meridional decay scale (e^{-1}) of kinetic energy is of order 3° (~330 km) of latitude whereas the downstream scale computed from Richardson's (1983) surface eddy kinetic energy measurements is closer to 10° of longitude (~800 km). The Reynolds stress term is positive south of the current and negative to the north reaching extrema within two degrees of the current's mean axis and then falling to small absolute values over several degrees much like the eddy kinetic energy. Webster (1961) first reported the tendency for negative values inshore of the Gulf Stream and noted that they implied a transfer of momentum from the eddies to the Stream—a kind of negative viscosity.

Probably the best examples of eddy-driven flows in the ocean general circulation are the recirculation cells found to the south (Worthington 1976) and north

* Contribution Number 6675 from the Woods Hole Oceanographic Institution.

Corresponding author address: Dr. Nelson Hogg, Woods Hole Oceanographic Institution, Woods Hole, MA 02543.

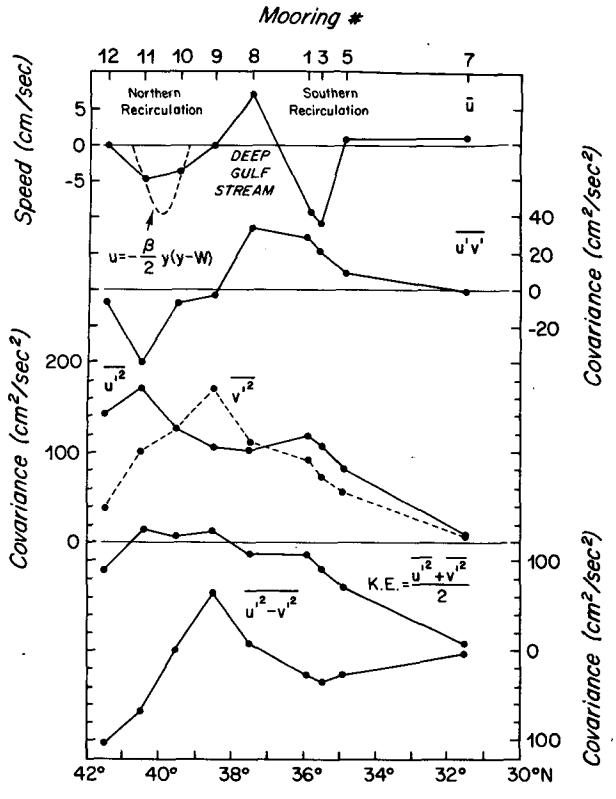

FIG. 1. Distributions of various covariance quantities from 55°W in the North Atlantic at 4000 m depth. The upper curve gives the mean zonal flow at 4000 m along with the predicted parabolic form arising from the imposition of uniform potential vorticity and the further requirement that it agree at moorings 10 and 11.

(Hogg 1983; Hogg et al. 1986) of the Gulf Stream (see upper panel of Fig. 1). Not only are these pronounced features of the real ocean but they result in most every eddy resolving numerical model of the general circulation, a particularly good example being the class of quasi-geostrophic models studied by Holland and Rhines (1980). There it was shown that the recirculations resulted from eddy vorticity fluxes, principally the so-called eddy thickness flux arising from rectification of eddies generated by baroclinic instability of the westward Sverdrup interior.

The influence of the eddies on the mean flow is best understood in terms of the mean vorticity balance which in its quasi-geostrophic form is

$$\bar{\mathbf{u}} \cdot \nabla \bar{q} = -\nabla \cdot \overline{\mathbf{u}'q'} \tag{1.1}$$

where q is the potential vorticity and $\mathbf{u}$ the horizontal velocity. The overbar indicates a temporal average and the prime a deviation from the average. The eddy vorticity flux, $\overline{\mathbf{u}'q'}$, in general has two components, a relative vorticity flux and a thickness flux which is not relevant to this barotropic analysis. The divergence of the former can be written:

$$\nabla \cdot \overline{\mathbf{u}'(v'_x - u'_y)}$$

$$= \left(\frac{\partial^2}{\partial x^2} - \frac{\partial^2}{\partial y^2}\right)\overline{u'v'} - \frac{\partial^2}{\partial x \partial y}(\overline{u'^2 - v'^2}). \tag{1.2}$$

Consider the distribution of $\langle \overline{u'v'} \rangle$ of Fig. 1 and the fact that meridional scales are much smaller than zonal. The divergence of the relative vorticity flux then becomes approximately:

$$\bar{\mathbf{u}} \cdot \nabla \bar{q} \approx \frac{\partial^2}{\partial y^2}\overline{u'v'} + \frac{\partial^2}{\partial x \partial y}(\overline{u'^2 - v'^2}) \tag{1.3}$$

the last term not being estimable from present data. However the curvature of $\overline{u'v'}$ just to the north of the Stream axis is positive.

If the mean advection term is dominated by the meridional advection of planetary vorticity and we use a planetary vorticity gradient of 3.6×10^{-11} m^{-1} s^{-1} (as enhanced by a positive bottom slope) then the Sverdrup-like balance yields a meridional mean flow of 4.0 mm s^{-1} from the curvature term for a maximum $|\overline{u'v'}|$ of 30 cm^2 s^{-2} distributed over a meridional scale of 150 km. Such a meridional flow, if spread over a zonal distance of 2000 km and a depth of 5 km would transport 40×10^6 m^3 s^{-1}—very similar to the amount of water estimated by Richardson (1985) to be carried in each of the two recirculations.

The very existence of an eddy vorticity flux divergence runs counter to various theoretical analyses which conclude that there should be no interaction between the eddy field and the mean flow (e.g., Boyd 1976). Thus, it is important to understand these distributions and how they arise.

Hogg and Stommel (1985) and, more recently, Ierley and Young (1988) have presented models in which the recirculation is determined by imposing the condition of homogenized, mean potential vorticity. In this case the ambient vorticity gradient vanishes and, ignoring the weaker zonal derivatives,

$$\bar{u}_{yy} = \beta \tag{1.4}$$

where β is the planetary vorticity gradient ($\beta \approx 3.6 \times 10^{-11}$ s^{-1} at 40°N, 55°W as augmented by the bottom slope). Double integration with the conditions that $\bar{u} = 0$ at $y = 0$ and $y = W$ gives

$$\bar{u}(y) = -\frac{\beta}{2} y(W - y). \tag{1.5}$$

If this parabolic form is fit to the mean zonal flows at moorings 10 and 11 in Fig. 1 so as to determine the width of the westward flow, W, we find that $W = 147$ km and the current has the shape shown by the dotted lines. Integration over W and a depth of $H = 5$ km gives a total recirculating transport of $H\beta W^3/12 = 48 \times 10^6$ m^3 s^{-1}, again not far from the Richardson (1985) value of 40×10^6 m^3 s^{-1} for the Northern Recirculation Gyre.

Of course, if the recirculation gyres are truly homogenized in potential vorticity then Eq. (1.1) would demand that the divergence of the eddy vorticity flux vanish and the Sverdrup-like balance discussed above would be inappropriate—the second term in the rhs of Eq. (1.3) must offset the first.

Stochastic models of Rossby wave generation with and without recirculations will be explored in the following sections and implications for the mean flow discussed.

2. Formulation

Motions near the Gulf Stream are only weakly depth dependent (Schmitz 1980; Hogg et al. 1986; Welsh et al. 1987). Although the Stream, itself, is strongly sheared its lateral movements appear to be quite barotropic (Halkin and Rossby 1985; Hall 1986). We will assume that motions exterior to the Stream are quasi-geostrophic and barotropic. The potential vorticity equation for small amplitude motions in a mean flow is (e.g., see Pedlosky 1979):

$$\left(\frac{\partial}{\partial t} + \bar{u}(y)\frac{\partial}{\partial x}\right)\nabla^2\psi + (\beta - \bar{u}''(y))\psi_x = 0 \quad (2.1)$$

where $\psi(\mathbf{x}, t)$ is the perturbation streamfunction from which the horizontal velocity components can be derived:

$$u = -\psi_y, \quad v = \psi_x. \quad (2.2)$$

In the conventional manner u and v are the east and north components of the perturbed velocity, f is the coriolis parameter, β its meridional derivative and $\bar{u}(y)$ is the mean flow which is taken to be zero or to satisfy the homogenized potential vorticity condition of Eq. (1.5).

We will assume that the motions are forced by the movement of a rigid boundary at the southern extremity of the domain whose configuration is $\eta(x, t)$ (see Fig. 2 for a conceptual picture). With the usual small amplitude assumption and a Taylor series expansion, this can be written as

$$v = \psi_x = \frac{\partial \eta}{\partial t} \text{ at } y = 0 \quad (\bar{u}(0) = 0). \quad (2.3)$$

Integrated once with respect to x, the condition on the streamfunction is

$$\psi = \int^x \frac{\partial \eta}{\partial t}\, dx \text{ at } y = 0. \quad (2.4)$$

The assumption of small amplitude motion is hardly justifiable but is a necessity to obtain a tractable mathematical problem. Effects of nonlinearities must await further numerical work such as that begun by Malanotte-Rizzoli et al. (1987).

These equations will be nondimensionalized using a lengthscale $L = 400 \text{ km}/2\pi \approx 64$ km determined by a meander wavelength. Appropriate time, T, velocity, V, streamfunction, P, and displacement, N, scales are given by

$$T = \frac{1}{\beta L}, \quad V = \beta L^2, \quad P = \beta L^3, \quad N = L.$$

The displacement function $\eta(x, t)$ is assumed to have two scales, one the length scale determined by the meanders and the other by their envelope which is more like 600 km. The ratio of these scales

$$\gamma = \frac{\text{Meander envelope scale}}{\text{Meander length scale}} = \frac{600}{64} = 9.4$$

will be assumed large with respect to unity. As the recirculation scale is zonally large and somehow related to the average effect of the eddies the width will be assumed to be of order 1 but change over a distance γ. Specifically,

$$W(x/\gamma) = \begin{cases} W_0(1 - x^2/\gamma^2), & |x| < \gamma \\ 0, & |x| > \gamma \end{cases} \quad (2.5)$$

where W_0 is the maximum width at $x = 0$. The nondimensional equations become

$$\left.\begin{aligned} &\nabla^2\psi = 0, \quad \bar{u}'' = \beta, \quad y < W(x/\gamma) \\ &\frac{\partial}{\partial t}\nabla^2\psi + \beta\psi_x = 0, \quad \bar{u} = 0, \quad y > W(x/\gamma) \end{aligned}\right\} \quad (2.6)$$

with

$$\psi = \int^x \frac{\partial \eta}{\partial t}\, dx, \quad y = 0,$$

all quantities being nondimensional. The solution for no recirculation can be obtained from the limit $W_0 \to 0$.

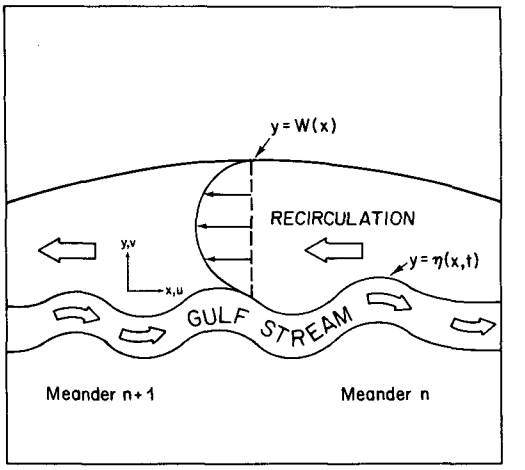

FIG. 2. A schematic view of the radiation problem showing two meanders in the Stream and the Northern Recirculation Gyre.

In principle, the variation in the width of the recirculation must be accompanied by both a zonal variation in the zonal velocity component and a mean meridional velocity. However, both of these effects will be $O(1/\gamma)$ and make no O(1) contribution to the vorticity balance. In the following analysis, an implicit two scaling procedure will be assumed in the x direction—a fast scale x and a slower one, x/γ. Only the lowest order will be retained.

We define the double Fourier transform of a function $\eta(x, t)$ and its inverse as follows:

$$\left.\begin{aligned}\hat{\eta}(k, \omega) &= \frac{1}{2\pi}\int\int \eta(x, t)e^{-i(kx-\omega t)}dxdt \\ \eta(x, t) &= \frac{1}{2\pi}\int\int \hat{\eta}(k, \omega)e^{i(kx-\omega t)}dkd\omega.\end{aligned}\right\} \quad (2.7)$$

Application to Eqs. (2.6) yields the following boundary value problem for a second-order ordinary differential equation in y:

$$\hat{\psi}(k, \omega, y, x/\gamma) = -G(k, y, x/\gamma)\frac{\omega}{k}\hat{\eta}(k, \omega) \quad (2.8)$$

with

$$\left.\begin{aligned}G_{yy}(k, y, x/\gamma) - k^2G(k, y, x/\gamma) = 0, \quad y < W(x/\gamma) \\ G_{yy} + l^2G = 0, \quad y > W(x/\gamma)\end{aligned}\right\} \quad (2.9)$$

$$l^2 = -k\left(k + \frac{1}{\omega}\right), \quad (2.10)$$

$$G(k, 0, x/\gamma) = 1 \text{ at } y = 0. \quad (2.11)$$

The solution is

$$G(k, y, x/\gamma) = \begin{cases} A_0(x/\gamma)e^{-ky} + A_1(x/\gamma)e^{+ky}, & y < W(x/\gamma) \\ A_2(x/\gamma)e^{-il(y-W)}, & y > W(x/\gamma)\end{cases} \quad (2.12)$$

using the radiation condition for $y > W$ to select the solution with outward energy flux for l real ($-1/\omega < k < 0$). If l is imaginary (i.e., $k > 0$ or $k < -1/\omega$) we set the imaginary part negative so that the solution decays away from the forcing. Contours of l in the (ω, k) plane are shown in Fig. 3. There is a limited region, $-1/\omega < k < 0$, in which l is real and free waves are possible.

Three conditions are needed to determine the $A_i(x/\gamma)$. Two are given by the condition (2.11) at $y = 0$ and the matching of the streamfunction at $y = W$. The third results from the matching of the tangential velocity as determined from a Taylor series expansion about $y = W$. It can be shown that

$$A_0 = \frac{\left(k + il + \frac{kW}{2\omega}\right)e^{kW}}{2k\cosh kW + \frac{kW}{\omega}\sinh kW + 2il\sinh kW}$$

$$A_1 = 1 - A_0 = \frac{\left(k - il - \frac{kW}{2\omega}\right)e^{-kW}}{2k\cosh kW + \frac{kW}{\omega}\sinh kW + 2il\sinh kW}$$

$$A_2 = \frac{2k}{2k\cosh kW + \frac{kW}{\omega}\sinh kW + 2il\sinh kW}$$

In general,

$$G(k, y, x/\gamma) = Ae^{i\phi(k,y,x/\gamma)} \quad (2.13)$$

where the amplitude and phase functions, $A(k, y, x/\gamma)$ and $\phi(k, y, x/\gamma)$, can be determined from the A_i above. For l imaginary the A_i and the function $G(k, y, x/\gamma)$ are all real and $\phi(k, y, x/\gamma)$ is zero.

In terms of the transform of the forcing function the horizontal velocity components are

$$\left.\begin{aligned}u = -\psi_y &= \frac{1}{2\pi}\int\int \left(\frac{\omega}{k}\right)\hat{\eta}(k, \omega)G_y e^{i(kx-\omega t)}dkd\omega \\ v = \psi_x &= -\frac{i}{2\pi}\int\int \omega\eta(k, \omega)Gke^{i(kx-\omega t)}dkd\omega\end{aligned}\right\}. \quad (2.14)$$

The ensemble averaged Reynolds stresses can be written:

$$\langle uu^*\rangle = \frac{1}{4\pi^2}\int\int\int\int F(k, k', \omega, \omega')G_y(k)G_y^*(k') \times e^{i[(k-k')x-(\omega-\omega')t]}dkdk'd\omega d\omega' \quad (2.15)$$

$$\langle vv^*\rangle = \frac{1}{4\pi^2}\int\int\int\int F(k, k', \omega, \omega')G(k)G^*(k') \times e^{i[(k-k')x-(\omega-\omega')t]}dkdk'd\omega d\omega' \quad (2.16)$$

$$\langle uv^*\rangle = \frac{i}{4\pi^2}\int\int\int\int F(k, k', \omega, \omega')G_y(k)G^*(k') \times k'e^{i[(k-k')x-(\omega-\omega')t]}dkdk'd\omega d\omega' \quad (2.17)$$

with

$$F(k, k', \omega, \omega') = \langle\hat{\eta}(k, \omega)\hat{\eta}^*(k', \omega')\rangle\frac{\omega}{k}\cdot\frac{\omega'}{k'}. \quad (2.18)$$

The asterisk indicates the complex conjugate while the angled brackets denote the ensemble average.

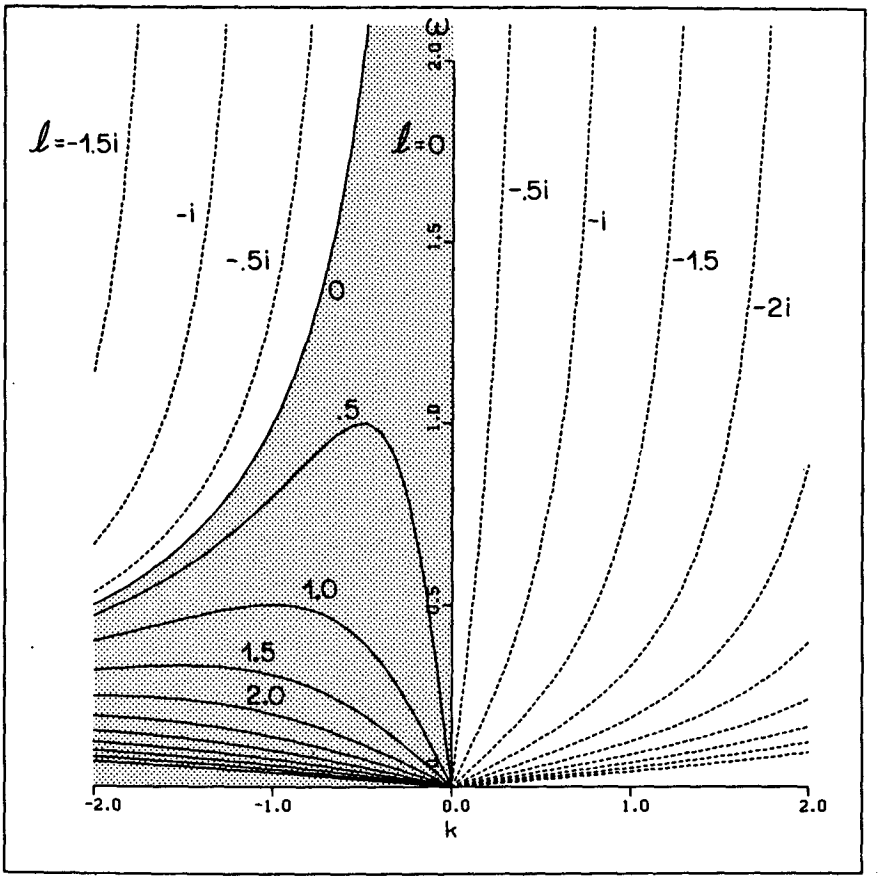

FIG. 3. Contours of the meridional wavenumber, l, in the (ω, k) plane. Solid curves in the shaded region are for the wave region, l real.

3. Stochastic forcing, $F(k, k', \omega, \omega')$

If a meander is considered to be a well defined event the displacement of the Stream is the sum over all of these events

$$\eta(x, t) = \sum_{n=1}^{N} \eta_n(x - x_n, t - t_n), \qquad (3.1)$$

with N tending toward infinity. Each meander has a different spatial and temporal origin (x_n, t_n). The double Fourier transform of (3.1) can be manipulated to show

$$\langle \hat{\eta}(k, \omega)\hat{\eta}^*(k', \omega') \rangle = \sum_{n=1}^{N} \langle e^{-i[(k-k')x_n-(\omega-\omega')t_n]}\hat{\eta}_n(k, \omega)\hat{\eta}_n^*(k', \omega') \rangle \qquad (3.2)$$

where the angled brackets indicate the stochastic average with respect to the various meander parameters and we have assumed that different meanders are independent.

The simplest assumption to make about the joint probability density function of the parameters is that they are all independent. Taking the probability density function for the temporal origin t_n to be uniformly distributed over a time T_N which also is very large

$$\langle e^{i(\omega-\omega')t_n} \rangle = \frac{1}{T_N} \int_{-T_N}^{0} e^{i(\omega-\omega')t_n} dt_n$$

$$= e^{-i(\omega-\omega')(T_N/2)} \frac{\sin(\omega - \omega')(T_N/2)}{T_N(\omega - \omega')}$$

which, for large T_N, becomes

$$\lim_{T_N \to \infty} \langle e^{i(\omega-\omega')t_n} \rangle = \frac{2\pi}{T_N} \delta(\omega - \omega'). \qquad (3.3)$$

The spatial origin, x_n, is not uniformly distributed. Surface eddy kinetic energy reaches a maximum near 65°W and one interpretation would be that meanders are more likely near this location. Taking the probability density function for x_n to be

$$p_r(x_n) = \frac{1}{\sqrt{2\pi}\gamma} e^{-x_n^2/2\gamma^2}$$

then

$$\langle e^{-i(k-k')x_n} \rangle = e^{-\gamma^2(k-k')^2/2} = \frac{\sqrt{2\pi}}{\gamma} D\left(\frac{\gamma}{\sqrt{2}}, k-k'\right) \tag{3.4}$$

where

$$D(q, x) \equiv \frac{q}{\sqrt{\pi}} e^{-q^2x^2} \tag{3.5}$$

defined so that in the limit of large q, $D(q, x) \to \delta(x)$. Therefore,

$$\lim_{\gamma\to\infty} \langle e^{-i(k-k')x_n} \rangle = \frac{\sqrt{2\pi}}{\gamma} \delta(k-k').$$

As opposed to the large T_N limit, however, γ is large but finite and it is important to retain the form of (3.4) so that,

$$F(k, k', \omega, \omega') = 4\pi^2 N_d \delta(\omega - \omega') \times D\left(\frac{\gamma}{\sqrt{2}}, k-k'\right) \langle \eta(k, \omega)\eta^*(k', \omega) \rangle \tag{3.6}$$

with

$$N_d = \lim_{N, T_N\to\infty} \frac{1}{\sqrt{2\pi}} \frac{N}{T_N\gamma}. \tag{3.7}$$

Here N_d can be thought of as the population density of meanders. The ratio N/T_N will become constant as T_N increases and can be evaluated as the number in existence at any one time, N_m, divided by their average lifetime. If we define the half lifetime to be T_l then

$$N_d \approx \frac{1}{\sqrt{8\pi}} \frac{N_m}{T_l\gamma}. \tag{3.8}$$

Discussion of the stochastic average with respect to meander shape parameters in Eq. (3.6) will be continued in section 4 and the Appendix.

When (3.6) and (2.13) are substituted into the covariances of Eqs. (2.15) to (2.17) then we have, for example,

$$\langle uv^* \rangle = iN_d \iiint D\left(\frac{\gamma}{2}, k-k'\right) k'A(k')[A_y(k) + iA(k)\phi_y(k)] e^{i[(k-k')x + (\phi(k) - \phi(k'))]} \times \langle \eta(\omega, k)\eta^*(\omega, k') \rangle \frac{\omega^2}{kk'} d\omega dk dk'. \tag{3.9}$$

For large γ contributions to the integrand will come from regions of (k, k', ω) space where $k \approx k'$. Therefore, we write

$$k' = k + \epsilon \tag{3.10}$$

and expand the other functions of k' in Taylor series. In particular,

$$\phi(k') = \phi(k) + \frac{\partial\phi}{\partial k}\epsilon \tag{3.11}$$

and Eq. (3.9) becomes, to lowest order in ϵ,

$$\langle uv^* \rangle \approx iN_d \iint kS(\omega, k) \cdot A(k)[A_y(k) + i\phi_y(k)A(k)] \times \int D\left(\frac{\gamma}{\sqrt{2}}, \epsilon\right) e^{-i\epsilon(x+\phi_k)} d\epsilon d\omega dk \tag{3.12}$$

where

$$S(\omega, k) \equiv \langle \eta(\omega, k)\eta^*(\omega, k) \rangle \frac{\omega^2}{k^2} \tag{3.13}$$

is the power spectral density of the streamfunction forcing function. The integral with respect to ϵ is easily evaluated as a Fourier transform with the result:

$$\langle uv^* \rangle \approx iN_d \iint kS(\omega, k)A(k)[A_y(k) + i\phi_y(k)A(k)] e^{-(x+\phi_k)^2/2\gamma^2} d\omega dk. \tag{3.14}$$

Only the real part of this expression has physical meaning:

$$\mathrm{Re}\langle uv^* \rangle \approx -N_d \iint kS(\omega, k) \times \phi_y A^2 e^{-(x+\phi_k)^2/2\gamma^2} d\omega dk \tag{3.15}$$

with similar expressions for $\langle uu^* \rangle$ and $\langle vv^* \rangle$:

$$\langle uu^* \rangle = N_d \iint S(\omega, k)(A_y^2 + \phi_y^2 A^2) \times e^{-(x+\phi_k)^2/2\gamma^2} d\omega dk \tag{3.16}$$

$$\langle vv^* \rangle = N_d \iint k^2 S(\omega, k) A^2 e^{-(x+\phi_k)^2/2\gamma^2} d\omega dk. \tag{3.17}$$

Just the Rossby wave portion of (ω, k) space has $\phi \neq 0$ and makes a contribution to the Reynolds stress quantity in (3.15). The whole domain contributes to the velocity variances but the trapped components, with imaginary l, will decay rapidly away from the forcing.

The quantity $x + \phi_k$ in the argument of the exponential governs the spatial dependence of the covariances. For the region exterior to the recirculation the wave components have phase $\phi = -l(y - W)$ and

$$x + \phi_k = x - \frac{dl}{dk}(y - W) = x + \frac{\omega_k}{\omega_l}(y - W). \tag{3.18}$$

Each (ω, k) component will propagate along group velocity rays and, thereby, reflect the zonal distribution of energy at $y = W$ (and, therefore, $y = 0$) along the meridians.

4. The meander forcing spectrum, $S(\omega, k)$

The most energetic Gulf Stream disturbances are meanders which have typical wavelengths of 400 km, peak to peak meridional displacements of 300 km and propagate to the east at 0.08 m s^{-1} (Cornillon, personal communication). Such motions, if considered as steadily propagating plane waves, cannot couple to the Rossby wave field as they would have zero energy in the appropriate part of frequency–wavenumber space. However, meanders are wavelike neither in space nor in time and are best thought of as transients. Consider the following form for the displacement $\eta(x, t)$ (illustrated in Fig. 4):

$$\eta(x, t) = ap(x - ct)g(t) \tag{4.1}$$

where a is the nondimensional amplitude ($a \approx 150$ km/64 km ≈ 2.3), $p(x - ct)$ gives the purely propagating form and $g(t)$ its growth and decay function. The propagation speed, $c \approx 0.54$, in nondimensional units. The double Fourier transform can be manipulated to give:

$$\hat{\eta}(k, \omega) = a\hat{p}(k)\hat{g}(kc - \omega). \tag{4.2}$$

For $p(x - ct)$ we choose the form with its Fourier transform (Fig. 4):

$$\left.\begin{aligned} p(x - ct) &= \frac{2(x - ct)}{\lambda} e^{1-2|x-ct|/\lambda} \\ \hat{p}(k) &= \left(\frac{2}{\pi}\right)^{1/2} \frac{8\lambda^2 ek}{(4 + \lambda^2 k^2)^2} \end{aligned}\right\}. \tag{4.3}$$

where λ is the meander half-wavelength (nondimensionally, $\lambda \approx \pi$). For time dependence we use the function:

$$g(t) = \frac{1}{2}\left[\tanh\left(\frac{t + T_l}{T_r}\right) - \tanh\left(\frac{t - T_l}{T_r}\right)\right] \tag{4.4}$$

$$\hat{g}(\sigma) = \left(\frac{\pi}{2}\right)^{1/2} \frac{T_r\sigma}{\sinh\left(\frac{\pi}{2} T_r\sigma\right)} \frac{\sin\sigma T_l}{\sigma}, \quad \sigma = \omega - kc, \tag{4.5}$$

which has two parameters, a formation/decay (half) time scale, T_r, and a half lifetime scale, T_l. These are both difficult to quantify but the meander lifetime is surely an order of magnitude greater than its formation time $2T_l \approx 10T_r$ which in turn is more likely to be O(1), $2T_r \approx 1$, say.

As T_l becomes very large $\hat{g}(\sigma) \to \sqrt{2\pi}\delta(\sigma)$, a line spectrum at the frequencies and wavenumbers which match the meander propagation rate, c. In this limit, not unexpectedly, no propagating waves are able to radiate into the recirculation. However, for finite T_l there is leakage into neighboring frequency–wavenumber bands and the transient response is not restricted to those waves which match the forcing phase speed.

The streamfunction forcing spectrum is now given by

$$\begin{aligned} S(k, \omega) &\approx \langle \eta(k, \omega)\eta^*(k, \omega)\rangle \left(\frac{\omega}{k}\right)^2 \\ &= \omega^2 \left\langle \left\{ a \frac{8\lambda^2 e}{(4 + \lambda^2 k^2)^2} \frac{\sin\sigma T_l}{\sigma} \frac{\sigma T_r}{\sinh\left(\frac{\pi}{2}\sigma T_r\right)} \right\}^2 \right\rangle \\ &\equiv \omega^2 \langle a^2 S_1(k; \lambda)\, S_2(\sigma; T_l)\, S_3(\sigma; T_r)\rangle \end{aligned} \tag{4.6}$$

where the ensemble average is with respect to the meander parameters a, λ, T_r and T_l. Equation (4.6) has been written as the product of three functions in order to isolate this parametric dependence. Each function attains a limiting maximum value as k or σ approach zero. The $S_2(\sigma; T_l)$ has periodically displaced zeros for higher σ but an ensemble average can be ex-

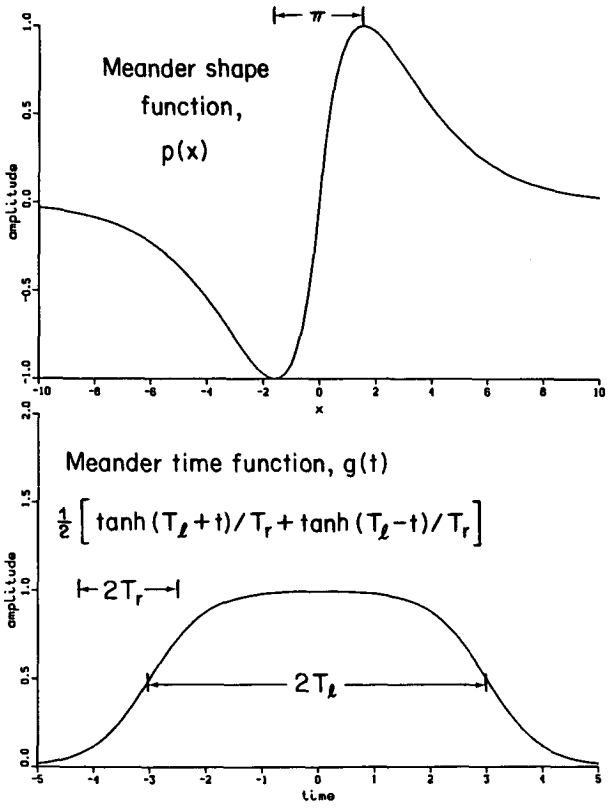

FIG. 4. Functional forms of the meander shape function $p(x)$ and growth-lifetime function $g(t)$.

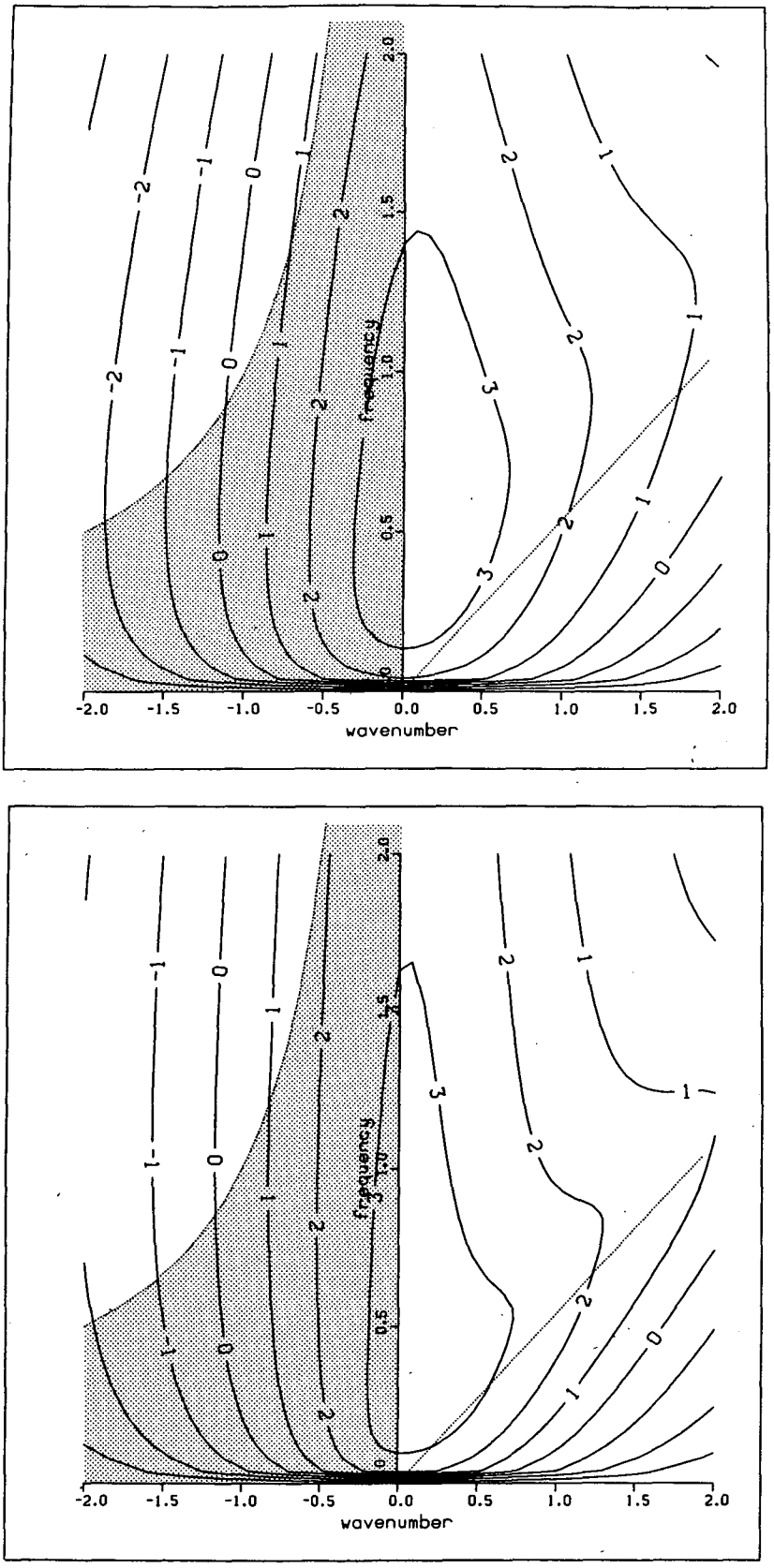

FIG. 5. The streamfunction forcing spectrum $\log_{10}S(\omega, k)$ for parameter values (a) $c = 0.54$, $T_r = 1$, $T_l = 3$ appropriate to the Northern Recirculation Gyre and (b) $c = 0.54$, $T_r = 0.5$ and $T_l = 6$. Freely propagating waves are possible in the shaded region.

pected to blur these zeros and make for a more monotonic dependence. In the Appendix it is argued that $\langle a^2 \rangle$ and the functions $\langle S_1(k; \lambda) \rangle$ and $\langle S_3(\sigma; T_r) \rangle$ can be used as defined in Eq. (4.6) provided that the average values of a, λ^{-1} and T_r^{-1} are substituted. $\langle S_2(\sigma; T_l) \rangle$ can be well approximated by:

$$\langle S_2(\sigma; T_l) \rangle \approx \langle T_l \rangle^2 \cdot \frac{1 + b(\langle T_l \rangle \sigma)^2}{1 + b(\langle T_l \rangle \sigma)^2 + 2b(\langle T_l \rangle \sigma)^4} \tag{4.7}$$

with $b = (4/\pi^2)(\pi^2 - 4)/(4 + \pi^2)$ chosen to give the proper value at the origin and the appropriate high wavenumber/frequency dependence. It is interesting to note that the function $\langle S_2(\sigma; T_l) \rangle$ increases as $\langle T_l \rangle^2$ for $\sigma = 0$ but is independent of $\langle T_l \rangle$ for large σ, i.e., in the Rossby wave regime away from the meander propagation speed line. In this limit the response will go as $\langle T_l \rangle^{-1}$ through the dependence of the population density, N_d [Eq. (3.8)].

The resulting frequency–wavenumber spectrum of the forcing is shown in Fig. 5. There is a peak along the line $\omega = \langle c \rangle k$ corresponding to the meander propagation rate. Although the spectral amplitude in the region where free Rossby waves can exist (shaded part of Fig. 5) is relatively insensitive to the meander lifetime parameter $\langle T_l \rangle$ it is quite sensitive to the rise time and the meander propagation speed $\langle c \rangle$. An example for different values of these two parameters is given in Fig. 5b.

5. Energy and Reynolds stress distributions

The various meander and general circulation parameters are summarized in Table 1. The most uncertain of these are the meander rise and lifetimes which have been chosen to give reasonable covariance amplitudes. The lifetime, in particular, $2\langle T_l \rangle = 6$ or 30 days might seem short, but should be viewed as the length of time a given meander travels without significant change of shape.

The covariances are computed by substituting Eq. (4.6) into Eqs. (3.15) to (3.17) and computing the double integrals numerically for a grid of x and y values. These are then contoured and the resulting two dimensional distributions are given in Fig. 6 for situations with and without a recirculation.

Even when integrated over the whole frequency–wavenumber spectrum there is a strong tendency for energy to move along group velocity lines. The maximum in the forcing at the boundary is carried to the northwest along a sloping trajectory: this is the essential ingredient which allows a meridional dependence to the Reynolds stresses.

Response at low wavenumbers and low frequencies is heavily favored (see Fig. 5). As these have much higher meridional wavenumber component than zonal, through geostrophy the zonal velocity component is much more energetic than the meridional. Although this is a feature of the observations away from the Stream (Fig. 1) the model contrast seems too large. If the meander wavenumber spectrum were broadened toward higher wavenumbers [by Eq. (4.6) it goes as k^{-8} for streamfunction] the ratio $\langle uu^* \rangle / \langle vv^* \rangle$ would decrease. However, these higher wavenumbers propagate more meridionally and would cause the meridional decay in the covariances to be weaker. It seems more likely that nonlinear and finite amplitude effects or inclusion of some frictional damping and more realistic geography are needed.

The effect of the recirculation is not substantial. Although magnitudes near the origin in the model with a recirculation are reduced by almost 50 percent over the model with no recirculation, comparable values are to be found in extrema displaced well to the northwest. The $\mathrm{Re}\langle uv^* \rangle$ covariance is the indicator of the Rossby wave motions which, according to this model, should be most intense to the northwest (and southwest) of the maximum meandering in the Gulf Stream. Contributions to $\langle uu^* \rangle$ and $\langle vv^* \rangle$ on the other hand are dominated by the trapped components and, consequently, reveal very little of the wave motions.

A direct comparison with the measured covariances at 55°W is made in Fig. 7. The computations of Fig. 6 were designed to simulate conditions for the Northern Recirculation Gyre. To the south of the Stream (at 55°W) the bottom becomes quite flat in the Sohm

TABLE 1. Model parameters (Bracketed values for southern recirculation).

Symbol	Meaning	Dimensional value	Nondimensional value
f	Coriolis parameter	9.3×10^{-5} s^{-1}	—
β	Effective planetary vorticity gradient	3.6×10^{-11} s^{-1} (1.8×10^{-11} s^{-1})	—
W_0	Maximum width of westward recirculation	147 km	2.3
γ	e-folding distance of meander energy	600 km	9.4
a	Maximum meander amplitude	150 km	2.3
λ	Meander half wavelength	200 km	π
c	Meander propagation speed	0.08 m s^{-1}	0.54 (1.08)
T_r	Meander half growth time	5 days	1 (0.5)
T_l	Meander half life time	15 days	3 (1.5)
N_m	Number of meanders	6	—

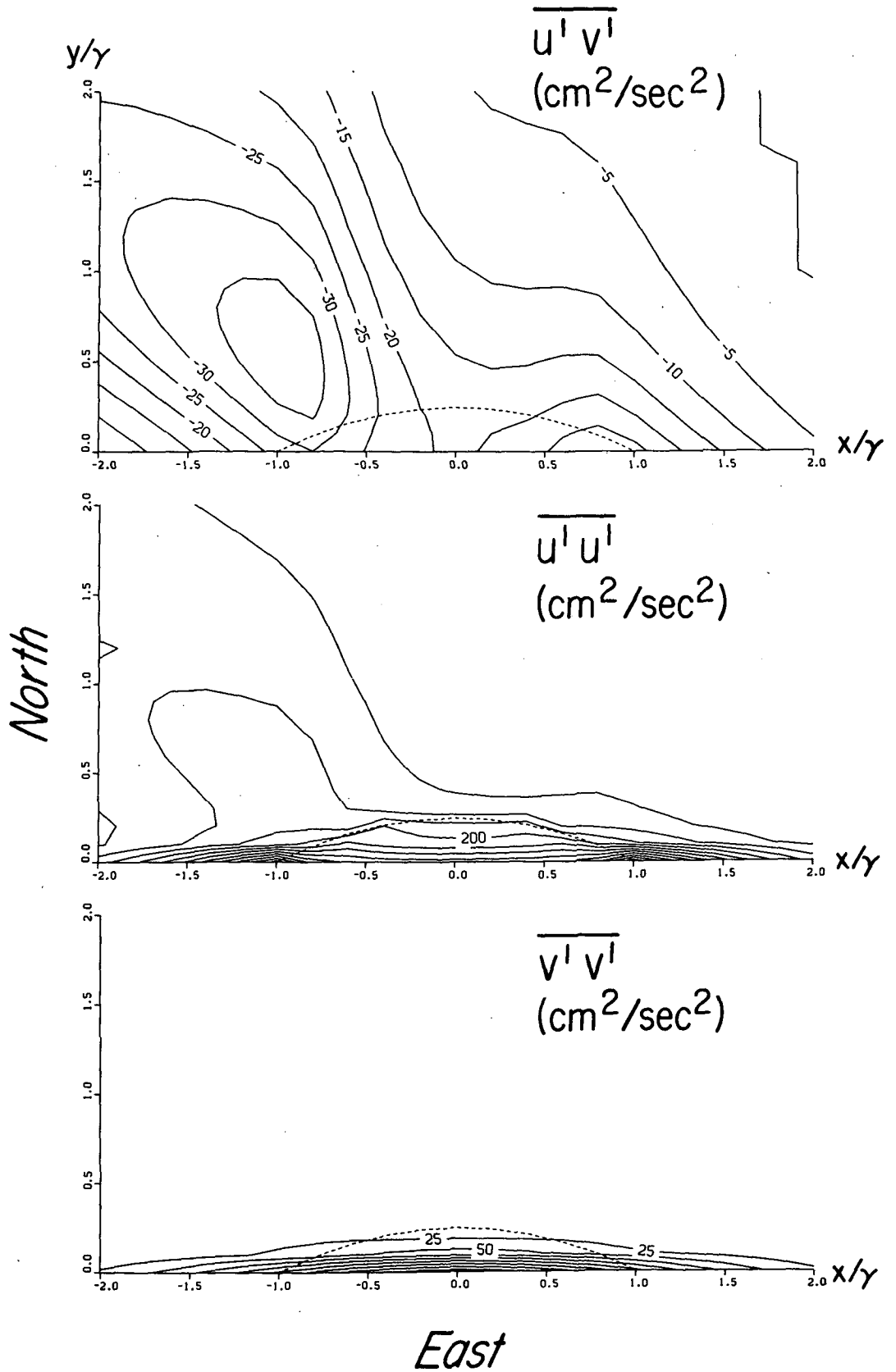

FIG. 6. Spatial distributions of velocity covariances for parameters appropriate to the Northern Recirculation Gyre. (a) With a recirculation, (b) without a recirculation.

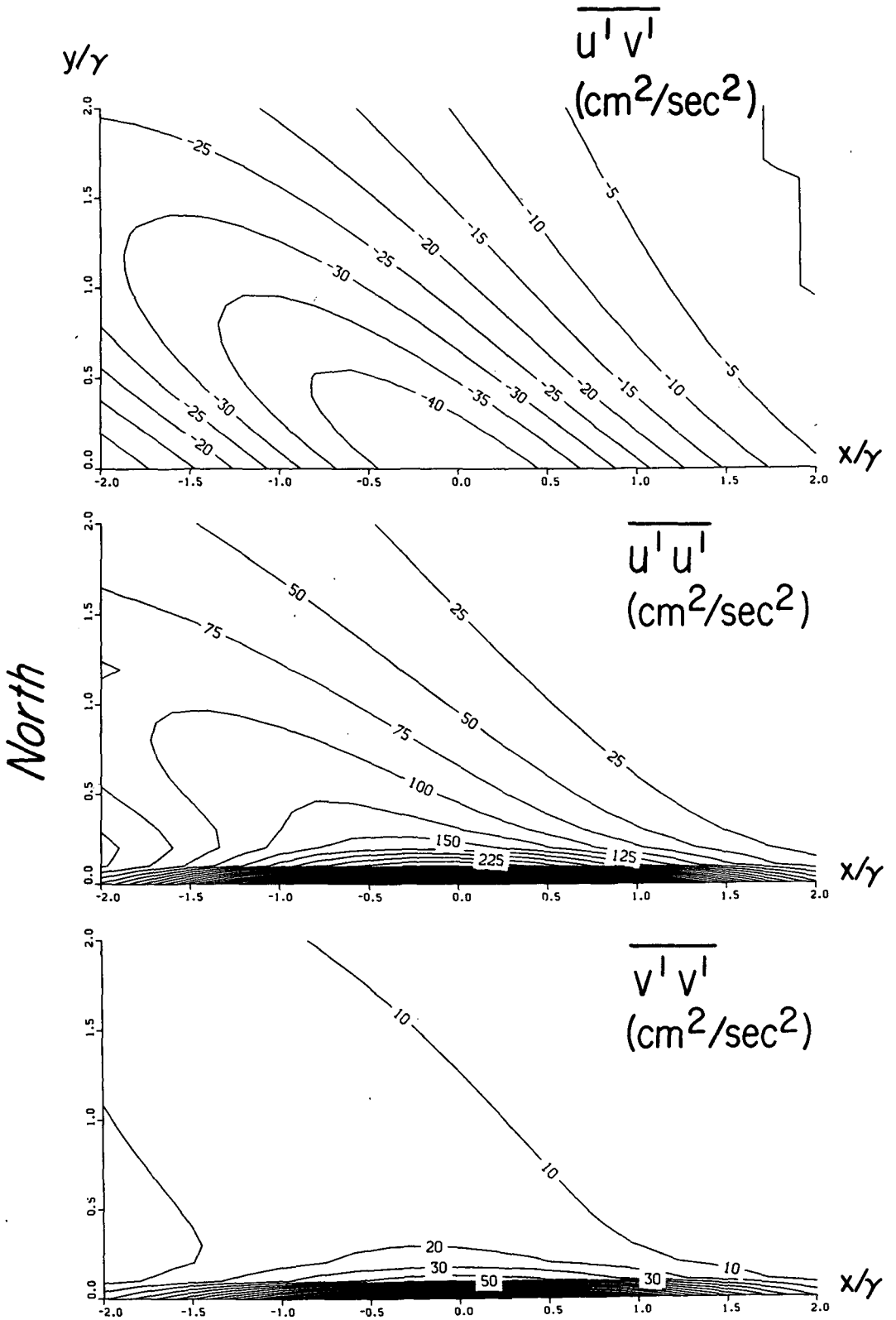

FIG. 6. (*Continued*)

Abyssal Plain so the value of β should be just that from the planetary gradient. Using a value one half that for the Northern Gyre decreases the velocity and increases time scales a factor of two so that the parameters c, T_r and T_l must be adjusted (bracketed values in Table 1).

The observations are from a longitude 600 km east of the maximum of the surface eddy kinetic energy but near where the maximum deep values are observed. In Fig. 7 computed meridional distributions from both longitudes are given. There is not much difference. Considering the simplified dynamics of the model the correspondence is encouraging.

6. Eddy–mean flow interactions

In the limit of $\gamma \to \infty$ both the recirculation and the meander forcing function will be independent of x, the spatial variations illustrated in Figs. 6 and 7 will disappear, and there will be no divergence of the eddy vorticity flux [Eq. (1.2)]. However, for γ finite the covariances have scales of variation of order γ and the eddy vorticity flux, being a second derivative quantity, is of order γ^{-2}.

In the region exterior to the recirculation the ambient potential vorticity gradient is β so the forced mean flow vorticity equation (1.1) becomes, in dimensional terms

$$\beta\bar{v} = \beta\bar{\psi}_x = \left(\frac{\partial^2}{\partial y^2} - \frac{\partial^2}{\partial x^2}\right)\overline{u'v'} + \frac{\partial^2}{\partial x \partial y}\,\overline{(u'^2 - v'^2)}, \qquad y > W(x/\gamma) \quad (6.1)$$

a modified Sverdrup balance. The wave vorticity flux terms can be obtained from differentiation of Eq. (3.15) to (3.17) and then integrated once with respect to x to obtain an integral expression for ψ which will be $O(1/\gamma)$.

Inside the recirculation the mean flow is specified by the homogeneous assumption and is given by Eq. (1.5) or

$$\bar{\psi} = -\frac{\beta}{12}(y - W)^2(2y + W), \quad y < W(x/\gamma). \qquad (6.2)$$

Because $\overline{u'^2}$ is discontinuous at $y = W(x/\gamma)$ in order to satisfy the matching condition there, the right-hand side of (6.1) is singular. However, the ambient potential vorticity gradient is also singular on this curve and one presumes that the mean vorticity equation remains in balance without singularities in the velocity field. Properly matching ψ across $y = W$ will necessitate the calculation of ψ in the recirculation to $O(1/\gamma)$ through investigation of the higher order vorticity balance. We have not done this but show, instead, in Fig. 8 the total transport streamfunction for the forced mean flow when there is no recirculation. The wave induced transport is on the order of a few Sverdrups mostly contained in a cyclonic gyre.

7. Summary and conclusions

We have shown that it is possible to reproduce meridional distributions of eddy kinetic energy and Reynolds stresses similar to those observed near the Gulf Stream through use of a rather simple, linear, stochastic model of wave forcing by a specified time dependent boundary. There are two important and required ingredients.

First, the boundary forcing must vary in intensity in the downstream direction. Waves propagate away along their ray paths and reflect the zonal distribution in the meridional direction.

Second, the forcing considered here comes from the meanders which dominate the Gulf Stream lateral displacements but generally travel eastward and, considered as steadily traveling features, cannot couple to westward moving Rossby waves. However, if their behavior is enriched to include growth and decay periods and a stochastic average is made with respect to their lifetimes spectral energy from the forcing "leaks" into the Rossby wave portion of the spectrum. For long lifetimes the forcing energy in this regime is actually independent of the lifetime parameter but strongly dependent on the meander propagation speed, growth/decay timescale, and amplitude.

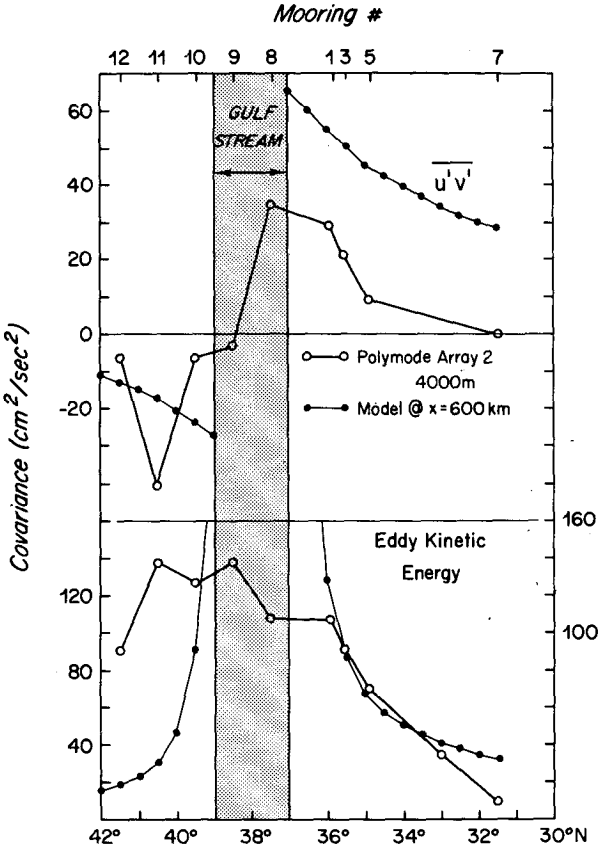

FIG. 7. A comparison between observed and computed covariance $\overline{u'v'}$ and eddy kinetic energy.

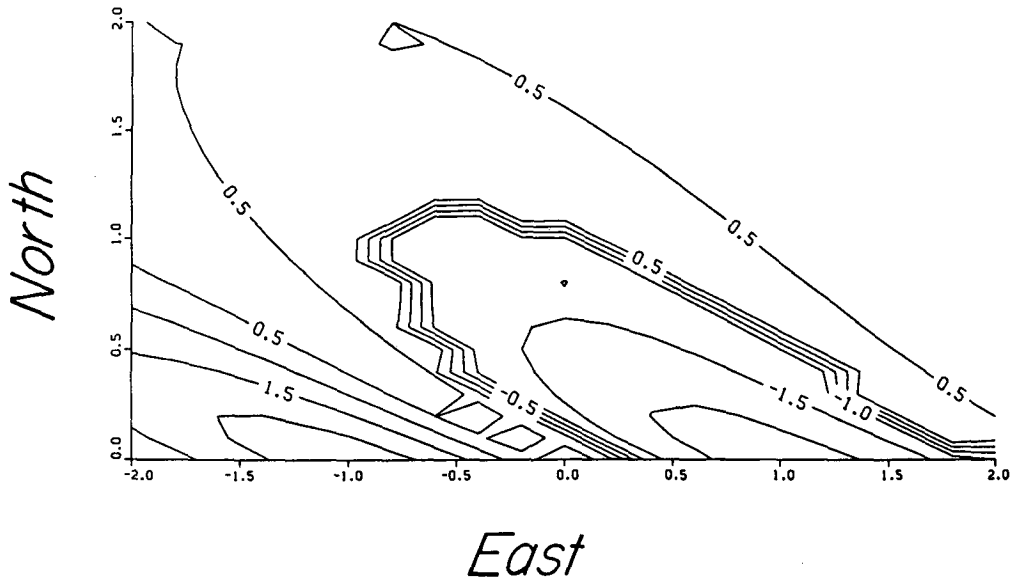

FIG. 8. The total transport streamfunction (in units of 10^6 m^3 s^{-1} assuming a depth of 5 km) for the case of no recirculation as forced by the wave generated vorticity flux divergence.

Although the intensity of low frequency motions is reproduced by this model, the rectification effects of these motions appears to be an order of magnitude too weak to force the recirculations found near the Gulf Stream.

There are a number of limitations of this theoretical study, some of which can be easily improved upon such as the inclusion of stratification and more general variations in the bottom topography (especially easy if they are just in the y direction). The real limitation, though, comes from the use of a linear model. In this region particle and phase velocities are similar in magnitude, and it is surprising that a linear model can do as well as it appears to do.

Acknowledgments. This work was generously supported by the Office of Naval Research through Contract N00014-85-C-0001, NR083-004 and the National Science Foundation through Grants OCE82-14925 and OCE86-08258. Careful reading by a reviewer helped to clarify the text.

APPENDIX

Stochastic Forcing

For this study the meanders are specified by a small number of parameters, in particular; wavelength λ, amplitude a, growth/decay time T_r, lifetime T_l, and propagation speed c. Taking them to be statistically independent the ensemble average becomes a product of ensemble averages with respect to the individual parameters. For example, the average with respect to amplitudes is

$$\langle a^2 \rangle = \frac{1}{2\epsilon} \int_{\langle a \rangle - \epsilon}^{\langle a \rangle + \epsilon} a^2 da$$

$$= \langle a \rangle^2 + \frac{1}{3} \epsilon^2$$

$$\approx \langle a \rangle^2 \qquad \text{(A1)}$$

for small ϵ. The meander lifetime parameter occurs in the function $S_2(\sigma; T_l)$ of equation (4.6):

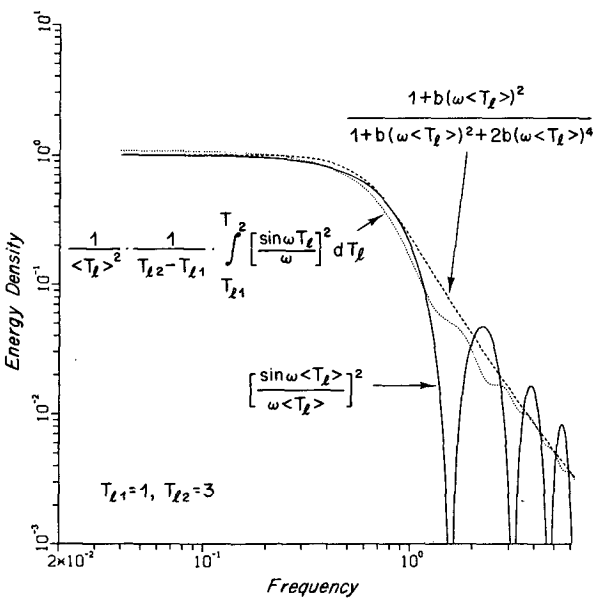

FIG. A1. Dependence of the stochastic average of the function $S_2(\sigma; T_l)$ on σ with the constant $b = (4/\pi^2)(\pi^2 - 4)/(\pi^2 + 4)$. The polynomial approximation was used.

$$\langle S_2(\sigma; T_l)\rangle = \frac{1}{2\epsilon}\int_{\langle T_l\rangle-\epsilon}^{\langle T_l\rangle+\epsilon}\left(\frac{\sin\sigma T_l}{\sigma}\right)^2 dT_l$$

$$= \frac{1}{2\sigma^2}\left[1 - \frac{\sin 2\sigma\epsilon\cos 2\sigma\langle T_l\rangle}{2\sigma\epsilon}\right] \quad \text{(A2)}$$

which takes the value $\langle T_l\rangle^2 + \epsilon^2/3$ at $\sigma = 0$ and falls as $0.5\sigma^{-2}$ for large σ. Figure A1 shows this dependence for $\langle T_l\rangle = 3$ and $\epsilon = 1.5$ along with the polynomial curve

$$\langle S_2(\sigma; T_l)\rangle \approx \langle T_l\rangle^2 \frac{1 + b(\sigma\langle T_l\rangle)^2}{1 + b(\sigma\langle T_l\rangle)^2 + 2b(\sigma\langle T_l\rangle)^4} \quad \text{(A3)}$$

where

$$b = \frac{4}{\pi^2}\left(\frac{\pi^2 - 4}{\pi^2 + 4}\right).$$

This agrees with (A2) at $\sigma = 0$ (for small ϵ) and large σ. It is noteworthy that, even though $S_2(\sigma; T_l)$ approaches a delta function for large T_l the amount of energy leaking into the $\sigma \neq 0$ region does not go to zero for the stochastic average and, in fact, becomes independent of $\langle T_l\rangle$.

The functions $S_1(k; \lambda)$ and $S_3(\sigma; T_r)$ are somewhat more straightforward as they are monotonic in k or σ. However, the variable $\sigma = \omega - ck$ contains the additional stochastic parameter c. In Fig. A2 are shown numerically determined averages for the product $\langle S_2(\sigma; T_l)S_3(\sigma; T_r)\rangle$ (as a function of ω and k) with respect to c, T_l, and T_r for independent uniform variations of ±50 percent in each parameter. In Fig. A3 the expected values of c and T_r^{-1} are used along with Eq. (A3). Although the average with respect to c leads to some spread of the contours near the line $\omega = \langle c\rangle k$ in Fig. A2 there is little dramatic change, especially in the wave regime and we shall use this form in section 4.

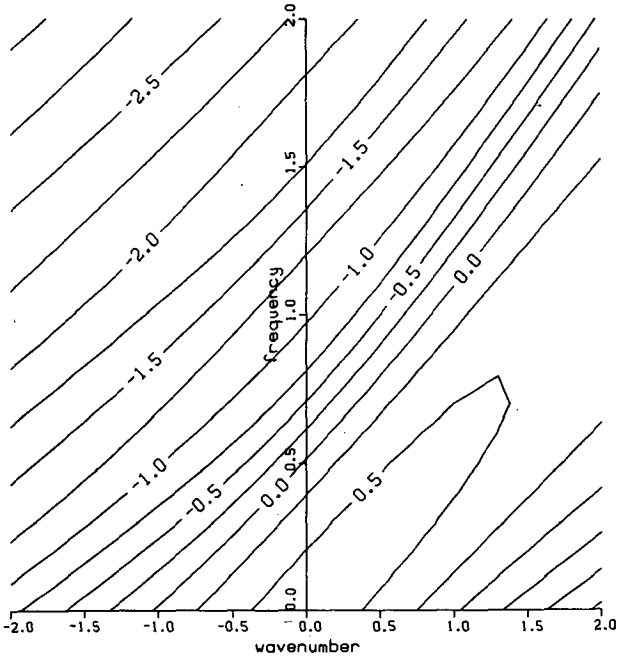

FIG. A2. The (ω, k) dependence of the stochastic average of $\langle S_2(\sigma; T_l)S_3(\sigma; T_r)\rangle$ over values of c, T_r, and T_l which are uniformly distributed over a range of ±50 percent (i.e., $0.54 < c < 0.81$, $0.5 < T_r < 1.5$, $1.5 < T_l < 4.5$).

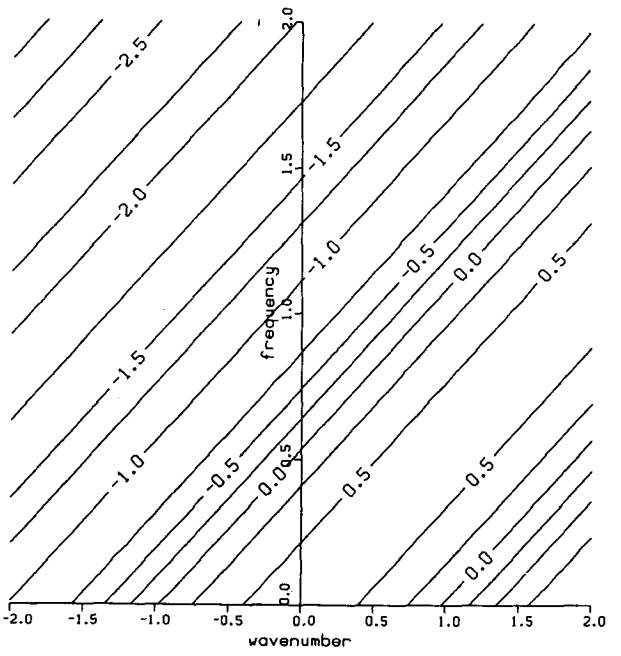

FIG. A3. As in Fig. A2 but with the expected values of c and T_r^{-1} used ($\langle c\rangle = 0.54$, $\langle T_r^{-1}\rangle = 0.75$).

REFERENCES

Boyd, J. P., 1976: The noninteraction of waves with the zonally averaged flow on a spherical earth and the interrelationships of eddy fluxes of energy, heat and momentum. *J. Atmos. Sci.*, **33**, 2285–2291.

Cheney, R. E., J. G. Marsh and B. D. Beckley, 1982: Global mesoscale variability from colinear tracks of SEASAT altimeter data. *J. Geophys. Res.*, **88**, 4343–4354.

Halkin, D., and T. Rossby, 1985: The structure and transport of the Gulf Stream at 73°W. *J. Phys. Oceanogr.*, **15**, 1439–1452.

Hall, M. M., 1986: Horizontal and vertical structure of the Gulf Stream velocity field at 68°W. *J. Phys. Oceanogr.*, **16**(11), 1814–1828.

Hogg, N. G., 1981: Topographic waves along 70°W on the Continental Rise. *J. Mar. Res.*, **39**, 627–649.

——, 1983: A note on the deep circulation of the western North Atlantic: Its nature and causes. *Deep-Sea Res.*, **30**, 945–961.

——, and H. Stommel, 1985: On the relationship between the deep circulation and the Gulf Stream. *Deep-Sea Res.*, **32**, 1181–1193.

——, R. S. Pickart, R. M. Hendry and W. Smethie, 1986: On the northern recirculation gyre of the Gulf Stream. *Deep-Sea Res.*, **33**(9A), 1139–1166.

Holland, W. R., and P. B. Rhines, 1980: An example of eddy-induced ocean circulation. *J. Phys. Oceanogr.*, **10**, 1010–1031.

Ierley, G., and W. R. Young, 1987: Nonlinear corner flows on a β-plane—A model of recirculation. Unpublished manuscript.

Louis, J. P., and P. C. Smith, 1982: The development of the barotropic radiation field of an eddy over a slope. *J. Phys. Oceanogr.*, **12**, 56–73.

Malanotte-Rizzoli, P., D. B. Haidvogel and R. E. Young, 1987: Nu-

merical simulation of transient boundary-forced radiation. Part 1: The linear regime. *J. Phys. Oceanogr.*, **17**, 1439–1457.

Pedlosky, J., 1977: On the radiation of mesoscale energy in the mid-ocean. *Deep-Sea Res.*, **24**, 591–600.

——, 1979: *Geophys. Fluid Dyn.*, Springer-Verlag, 624 pp.

Price, J. F., and H. T. Rossby, 1982: Observations of a barotropic planetary wave in the western North Atlantic. *J. Mar. Res.*, **40**(Suppl.), 543–558.

Richardson, P. L., 1983: Eddy kinetic energy in the North Atlantic form surface drifters. *J. Geophys. Res.*, **88**(C7), 4355–4367.

——, 1985: Average velocity and transport of the Gulf Stream near 55°W. *J. Mar. Res.*, **43**(1), 83–111.

Schmitz, W. J., Jr., 1980: Weakly depth-dependent segments of the North Atlantic circulation. *J. Mar. Res.*, **38**, 111–133.

——, 1984: Abyssal eddy kinetic energy in the North Atlantic. *J. Mar. Res.*, **42**(3), 509–536.

Talley, L. D., 1983: Radiating barotropic instability. *J. Phys. Oceanogr.*, **13**, 972–987.

Weatherly, G. L., and E. A. Kelly, 1985: Storms and flow reversals at the HEBBLE site. *Mar. Geol.*, **66**, 205–218.

Webster, F., 1961: The effect of meanders on the kinetic energy balance of the Gulf Stream. *Tellus*, **13**, 392–401.

Welsh, E. B., N. G. Hogg and R. M. Hendry, 1987: The relationship of low frequency deep variability near the HEBBLE site to Gulf Stream fluctuations. Unpublished manuscript.

Worthington, L. V., 1976: On the North Atlantic Circulation. *The Johns Hopkins Oceanographic Studies*, **6**, 110 pp.